Microsyst Technol (2017) 23:2931–2942
DOI 10.1007/s00542-016-3094-x

TECHNICAL PAPER

Modeling the effect of microstructure on the coupled torsion/bending instability of rotational nano-mirror in Casimir regime

M. Keivani[1] · A. Koochi[2] · J. Mokhtari[3] · N. Abadian[3] · M. Abadyan[2]

Received: 29 April 2016 / Accepted: 28 July 2016 / Published online: 8 August 2016
© Springer-Verlag Berlin Heidelberg 2016

Abstract It has been well-established that the physical performance of nano-devices might be affected by the microstructure. Herein, a 2-degree-of-freedom model based on the modified couple stress elasticity is developed to incorporate the impact of microstructure in the torsion/bending coupled instability of rotational nano-electromechanical mirror. The governing equation of the mirror is derived incorporating the effects of electrostatic Coulomb and corrected Casimir forces with the consideration of the finite conductivity of interacting surfaces. Effect of microstructure-dependency on the instability parameters are determined as a function of the microstructure parameter, bending/torsion coupling ratio, vacuum fluctuation parameter and geometrical dimensions. It is found that the bending/torsion coupling substantially affects the stable behavior of the mirrors especially those with long rotational beam elements. Depending on the geometry and material characteristics, the presented model is able to simulate both hardening behavior (due to microstructure) and softening behavior (due to torsion/bending coupling) of the nano-mirror.

✉ M. Abadyan
abadyan@yahoo.com

[1] Shahrekord University of Medical Sciences, Shahrekord, Iran

[2] Shahrekord Branch, Islamic Azad University, Shahrekord, Iran

[3] Department of Mathematics, Isfahan (Khorasgan) Branch, Islamic Azad University, Isfahan, Iran

1 Introduction

During the recent decades, ultra-small devices have greatly influenced various branches of sciences including nanophotonics and optoelectronics. Among the ultra-small devices, rotational micro/nano-mirrors have been increasingly used in developing nano-electromechanical systems (NEMS) nano-/micro-opto-electromechanical systems (NOEMS/MOEMS) (Toshiyoshi and Fujita 1996; Ford et al. 1999). The rotational mirrors are utilized as essential elements in fabrication of optical switches, light modulators, etc. Fig. 1 shows the schematic of a typical rotational micro/nano-mirror that is constructed from a movable mirror suspended above fixed conductive ground electrode. The movable component is a main-plate (mirror) attached to two supporting rotational beams. The fixed component is a conductive exciting electrode which is fixed above a substrate. By imposing a DC voltage differential between the components the main-plane deflects and rotates, simultaneously. At a critical voltage, i.e., the pull-in voltage, the Coulomb torque/force exceeds the elastic resistance and the mirror adheres the fixed plane. Predicting the pull-in threshold is crucial for design and fabrication of the torsional mirrors. In this regard, many investigators have focused on modeling the instability and determining the pull-in parameters of rotational systems (Zhao et al. 2005; Moeenfard and Ahmadian 2013; Xiao et al. 2001; Degani and Nemirovsky 2002). Previous researchers have developed one-degree-of-freedom (1-DOF) to capture the pull-in parameters of torsional mirrors (Nemirovsky and Bochobza-Degani 2001; Degani et al. 1998; Moeenfard et al. 2012; Zhang et al. 2001; Wen-Hui and Ya-Pu 2003; Guo and Zhao 2006; Beni and Abadyan 2013). Degani et al. (1998) studied the pull-in instability rotational micro-mirror by using a 1-DOF model and compared the obtained

results with the experimental measurement. The 1-DOF model has incorporated only the torsional instability mode, thus, are reliable only if the deflection of the mirror is negligible. However, when the torsional-induced displacement and vertical deflection of the mirror are of the same order, the pull-in parameters could not be accurately computed via 1-DOF models. In this case bending and stretching of the supporting beams should be taken into account as well as torsion. In this regard, other investigators have employed 2-DOF models to calculate the coupling between the bending and torsion instability of the rotational systems (Bochobza-Degani and Nemirovsky 2002; Huang et al. 2004; Rezazadeh et al. 2007; Daqaq et al. 2008; Beni et al. 2012; Moeenfard and Ahmadian 2013).

The scale dependency of material properties at small scale is an important phenomenon that might be crucial in ultra-small systems. If the characteristic dimension of metallic components be of the order of the intrinsic material length scale, a hardening trend in the mechanical characteristics of the components appears. Fleck et al. (1994) has been observed the microstructure-dependent response of some materials in torsional loading. Therefore, the microstructure is considered as an important phenomenon that might affect the stable behavior of rotational mirrors. This microstructure-dependency of material characteristics can be modeled using size-dependent theories such as modified couple stress theory (MCST) (Yang et al. 2002), nonlocal elasticity (Eringen 1983; Sedighi 2014; Miandoab et al. 2015) and strain gradient theory (Lam et al. 2003; Sedighi et al. 2014, Akgoz and Civalek 2015a; Peng et al. 2015) which incorporated the small-size effects in the governing equations can be employed. Akgoz and Civalek employed the strain gradient theory to study the Shear deformation of functionally graded microbeams (Akgöz and Civalek 2014a) and the longitudinal free vibration of micro beams(Akgoz and Civalek 2014b). Among the size-dependent theories, the MCST is extensively used to describe the size-dependent behavior of beam-type structures (Akgoz and Civalek 2011a, b; Abdi et al. 2011; Rahaeifard et al. 2011; Beni et al. 2011) due to the high accuracy, low number of additional constants and the convenience of application. For example while strain gradient theory need three martial scale properties (Akgoz and Civalek 2015b), the MCST has only one material length scale parameter (Koochi et al. 2015). In recent years, the MCST has been employed for modeling the microstructure-dependent instability of rotational actuators (Beni 2015).

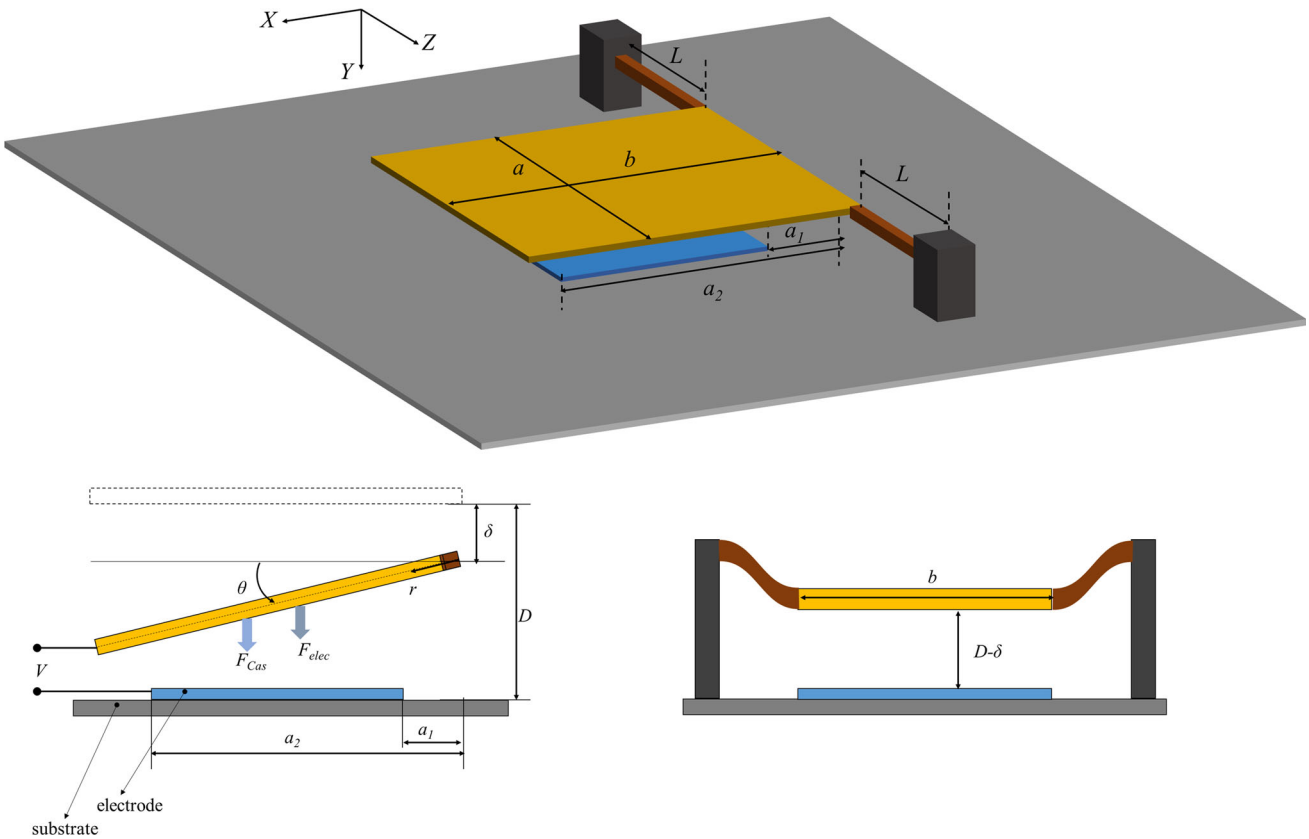

Fig. 1 Schematic diagram of rotational nano-mirror

Another phenomenon which can significantly affect the behavior of ultra-small structures is the presence of dispersion forces, i.e., van der Waals interaction and Casimir force. Although the dispersion forces force can be ignored in designing micro-scale actuators, it plays crucial role at submicron (Lin and Zhao 2003). The Casimir force appears when the distance between the two interacting bodies is so large that the virtual photons emitted by atoms of one body cannot reach the second body during its lifetime (Lin and Zhao 2007a). The effects of Casimir force on the static and dynamic behavior of nano-devices and NEMS structures have been investigated theoretically and experimentally by several researchers in the last decade (Lin and Zhao 2005, 2007b; Batra et al. 2007; Buks and Roukes 2001). A 1-DOF model for predicting the influence of Casimir and van der Waals forces on the pull-in instability of nano-mirror is presented by Guo and Zaho (2004). Duan and Rach (2013) demonstrated that if the distance between the movable components in NEMS devices they considered becomes less than 100 nm, they stick together due to strong Casimir force. It was demonstrated that the strength of vacuum fluctuation between two different bodies significantly depends on the material characteristics of the interacting surfaces (Lamoreaux 2004; Noruzifar et al. 2011). For the first time, Hargraves (1965) and Bezerra et al. (1997) presented the modification of Casimir attraction due to finite conductivity of the interacting flat plates. These investigators have introduced the simple approximations for correction of Casimir force as a function of plasma frequency of material. In this paper and in order to achieve the precise modeling of Casimir force, the effect of finite conductivity of the materials which verified by experimental measurements (Capasso et al. 2007; Rodriguez et al. 2011) is taken into account.

To the best knowledge of the authors, none of the previous researchers has incorporated the influence of microstructure effect in 2-DOF models used for simulating the rotational nano/micromirrors. Therefore, the authors present a new microstructure dependent two-degree-of-freedom (2-DOF) model to incorporate the size phenomena in the torsion–bending coupled instability of rotational NEMS mirror. In addition, the influence of Casimir force by considering the effect of finite conductivity of the materials has been incorporated in the model.

2 Fundamentals of MCST

Using the MCST, the strain energy U in region Ω is shown (Yang et al. 2002)

$$U = \frac{1}{2}\int_{\Omega}\left(\sigma_{ij}\varepsilon_{ij} + m_{ij}\chi_{ij}\right)dV, \tag{1}$$

where, the stress tensor σ_{ij}, strain tensor ε_{ij}, deviatoric part of the couple stress tensor m_{ij} and symmetric curvature tensor χ_{ij} are defined by

$$\sigma_{ij} = \lambda tr(\varepsilon_{ij})I + 2\mu\varepsilon_{ij}, \tag{2a}$$

$$\varepsilon_{ij} = \frac{1}{2}\left((\nabla u)_i + (\nabla u)_i^T\right), \tag{2b}$$

$$m_{ij} = 2l^2\mu\chi_{ij}, \tag{2c}$$

$$\chi_{ij} = \frac{1}{2}\left((\nabla\theta)_i + (\nabla\theta)_i^T\right), \tag{2d}$$

$$\theta_i = \frac{1}{2}(curl(\mathbf{u}))_i, \tag{2e}$$

where μ, λ, l, r and θ are shear modulus, Lame constant, length scale parameter, displacement vector and rotation vector, respectively. It should be noted that the Lame constant λ, can be explained as:

$$\lambda = \frac{E\upsilon}{(1+\upsilon)(1-2\upsilon)}, \tag{3}$$

where E is Young's modulus and υ is Poisson's ratio.

3 Governing equations

As shown in Fig. 1, the mirror is modeled by a moveable main-plate suspended by two nano-beams over a fixed substrate electrode. In order to derive the equilibrium equations, it is required to compute the electrical and Casimie forces (F_{elec} and F_{Cas}) and moments (M_{elec} and M_{Cas}) acting on the main plate.

3.1 Calculating of electrical force and moment

The electrical force of a differential element of the main-plate (dF_{elec}) can be written as (Beni et al. 2012)

$$dF_{elec} = \frac{\varepsilon b V^2}{2(D-\delta-r\sin(\theta))^2}dr, \tag{4}$$

where θ and δ are the rotation and deflection of main-plate. In the above equation ε is permittivity and V is applied voltage. Using Eq. (4), the total electrical force (F_{elec}) is obtained as:

$$F_{elec} = \int_{a_1}^{a_2} dF_{elec} = \frac{\varepsilon V^2 b}{2\sin(\theta)}\left(\frac{1}{D-\delta-a_2\sin(\theta)} - \frac{1}{D-\delta-a_1\sin(\theta)}\right). \tag{5}$$

By applying $\sin(\theta)\approx\theta$, $\theta_{\max} = \frac{D}{a}$, $\Delta = \frac{\delta}{D}$, $\Theta = \frac{\theta}{\theta_{\max}}$, $\alpha = \frac{a_1}{a}$ and $\beta = \frac{a_2}{a}$ in Eq. (5), the electrical force can be simplified as:

$$F_{elec} = \frac{\varepsilon V^2 b}{2\theta_{\max}\Theta D}\left\{\frac{1}{1-\Delta-\beta\Theta} - \frac{1}{1-\Delta-\alpha\Theta}\right\}. \quad (6)$$

By using Eq. (4) the electric moment (dM_{elec}) can be explained as:

$$dM_{elec} = \frac{\varepsilon b V^2}{2(D-\delta-r\sin(\theta))^2} r\cos(\theta)dr. \quad (7)$$

Hence, the total electric moment (M_{elec}) is defined as:

$$M_{elec} = \int_{a_1}^{a_2} dM_{elec} = \frac{\varepsilon V^2 b\cos(\theta)}{2\sin^2\theta}\left\{\frac{D-\delta}{D-\delta-a_2\sin\theta} - \frac{D-\delta}{D-\delta-a_1\sin\theta} + \ln\left(\frac{D-\delta-a_2\sin\theta}{D-\delta-a_1\sin\theta}\right)\right\}. \quad (8)$$

Using dimensionless parameters and assuming $\sin(\theta) \approx \theta$ and $Cos(\theta) \approx 1$, Eq. (8) can be rewritten as:

$$M_{elec} = \frac{\varepsilon b V^2}{2\Theta^2\theta_{\max}^2}\left\{\frac{1-\Delta}{1-\Delta-\beta\Theta} - \frac{1-\Delta}{1-\Delta-\alpha\Theta} + \ln\left[\frac{1-\Delta-\beta\Theta}{1-\Delta-\alpha\Theta}\right]\right\}. \quad (9)$$

3.2 Calculating of Casimir force and moment

Lambrecht et al. (1997) demonstrated that due to frequency-dependent reflectivity of finite conductive materials, the Casimir attraction between mirrors is always smaller than that between perfect conductive reflectors. To express the corrected formulation for Casimir force in finite conductive materials more precisely, the following second order modified relations for the differential forces can be employed (Lamoreaux 1999):

$$dF_{Cas} = \frac{\pi^2\hbar c b}{240(D-\delta-r\sin(\theta))^4}\left(1 - \frac{16c}{3\omega_p(D-\delta-r\sin(\theta))} + \frac{24c^2}{\omega_p^2(D-\delta-r\sin(\theta))^2}\right)dr, \quad (10)$$

where $\hbar$ is Planck's constant divided by 2π, and c is the light speed. By integrating Eq. (10), the total Casimir force (F_{Cas}) applied on main-plate is obtained as:

$$F_{Cas} = \int_0^a dF_{Cas} = \frac{\pi^2\hbar c a b}{1440(D-\delta)^3(D-\delta-a\sin\theta)^3}\left\{2a^2\sin^2\theta + 6(D-\delta)(D-\delta-a\sin\theta) - \frac{8c(2D-2\delta-a\sin\theta)}{\omega_p}\left[\frac{D-\delta-a\sin\theta}{D-\delta} + \frac{D-\delta}{D-\delta-a\sin\theta}\right] + \frac{144c^2}{\omega_p^2}\left[\frac{D-\delta-a\sin\theta}{D-\delta} + \frac{a\sin\theta}{D-\delta-a\sin\theta} + \frac{a^4\sin^4\theta}{5(D-\delta)^2(D-\delta-a\sin\theta)^2}\right]\right\} \quad (11)$$

Using dimensionless parameters, Eq. (11) can be rewritten as

$$F_{Cas} = \frac{\pi^2\hbar c a b}{1440D^4(1-\Delta)^3(1-\Delta-\Theta)^3} \times \left\{2\Theta^2 + 6(1-\Delta)(1-\Delta-\Theta) - \frac{8c(2-2\Delta-\Theta)}{D\omega_p} \times \left[\frac{1-\Delta-\Theta}{1-\Delta} + \frac{1-\Delta}{1-\Delta-\Theta}\right] + \frac{144c^2}{D^2\omega_p^2}\left[\frac{1-\Delta-\Theta}{1-\Delta} + \frac{\Theta}{1-\Delta-\Theta} + \frac{\Theta^4}{5(1-\Delta)^2(1-\Delta-\Theta)^2}\right]\right\}. \quad (12)$$

By using Eq. (10) the Casimir acting on a differential element of the main-plate (dM_{Cas}) can be written as:

$$dM_{Cas} = \frac{\pi^2\hbar c b}{240(D-\delta-r\sin(\theta))^4}\left(1 - \frac{16c}{3\omega_p(D-\delta-r\sin(\theta))} + \frac{24c^2}{\omega_p^2(D-\delta-r\sin(\theta))^2}\right)r\cos(\theta)dr. \quad (13)$$

By integrating Eq. (13), the Casimir moment applied on the main-plate (M_{cas}) is

$$M_{Cas} = \int_0^a dM_{Cas} = \frac{\pi^2\hbar c b a^2\cos(\theta)}{1440(D-\delta)^3(D-\delta-a\sin\theta)^3}\left\{(D-\delta)(3D-3\delta-a\sin\theta) - \frac{8c[2(D-\delta)^2 + (2D-2\delta-a\sin\theta)^2]}{3\omega_p(D-\delta-a\sin\theta)} + \frac{72c^2}{\omega_p^2}\left(\frac{D-\delta}{D-\delta-a\sin\theta} + \frac{a^2\sin^2\theta(5D-5\delta-a\sin\theta)}{10(D-\delta)(D-\delta-a\sin\theta)^2}\right)\right\}. \quad (14)$$

Using dimensionless parameters and assuming $\sin(\theta) \approx \theta$ and $Cos(\theta) \approx 1$, Eq. (14) can be rewritten as

$$M_{Cas} = \frac{\pi^2\hbar c b a^2}{1440D^4(1-\Delta)^3(1-\Delta-\Theta)^3}\left\{(1-\Delta)(3-3\Delta-\Theta) - \frac{8c[2(1-\Delta)^2 + (2-2\Delta-\Theta)^2]}{3D\omega_p(1-\Delta-\Theta)} + \frac{72c^2}{D^2\omega_p^2}\left(\frac{D-\delta}{1-\Delta-\Theta} + \frac{\Theta^2(5-5\Delta-\Theta)}{10(1-\Delta)(1-\Delta-\Theta)^2}\right)\right\}. \quad (15)$$

It should be noted that, the beams have torsion and deflection simultaneously. In the following, the superposition principal is applied to derive the torsion and bending equilibrium of the rotational mirror.

3.3 Torsion equilibrium of the beam

Considering the same geometry for nanobeams, one can obtain the following equation for each nanobeam:

$$\frac{1}{2}(M_{elec}+M_{Cas})-M_{elas}=0. \tag{16}$$

In above relation M_{elas} is the torsional elastic resistance moment of each nano-beam.In order to calculate the elastic moment M_{elas} of the nanobeam based on the MCST, one can start with the Saint–Venant's approach and assume the displacement field as (Dym and Shames 1984):

$$\begin{aligned} u_1 &= -\Omega YZ \\ u_2 &= -\Omega XZ \\ u_3 &= \Omega\psi(X,Y), \end{aligned} \tag{17}$$

where u_1, u_2 and u_3 are the displacement along the X,Y and Z direction, respectively. Furthermore, Ω is the angle of twist per unit length along the beam and the function $\psi(X,Y)$ is the warping function depending on X and Y only.

The governing equation of the torsional bar based on the MCST can be obtained as (see Tong et al. 2004; Tsiatas and Katsikadelis 2011 for details):

$$\frac{l^2}{4}\frac{\partial^4\Phi}{\partial X^4}+\frac{l^2}{4}\frac{\partial^4\Phi}{\partial Y^4}+\frac{l^2}{2}\frac{\partial^4\Phi}{\partial X^2\partial Y^2}-\frac{\partial^2\Phi}{\partial X^2}-\frac{\partial^2\Phi}{\partial Y^2}=0 \tag{18}$$

with the boundary conditions of:

$$\begin{aligned} &\frac{\partial\Phi}{\partial n}-\frac{l^2}{4}\frac{\partial^3\Phi}{\partial n^3}-\frac{l^2}{2}\frac{\partial^3\Phi}{\partial n\partial s^2}+\frac{l^2}{2}\frac{\partial}{\partial s}\left(\frac{1}{\rho}\frac{\partial\Phi}{\partial s}\right)-n_X Y+n_Y X=0, \\ &\frac{\partial^2\Phi}{\partial n^2}-\frac{\partial^2\Phi}{\partial s^2}-\frac{2}{\rho}\frac{\partial\Phi}{\partial n}=0. \end{aligned} \tag{19}$$

In the above relations, ρ, n(n_x,n_y) and s($-n_y$,n_x) are the curvature, the unit (outward) vector normal to the boundary and the unit tangent to the boundary, respectively (Tong et al. 2004; Tsiatas and Katsikadelis 2011). Finally, the elastic moment of the beam can be determined as the following:

$$M_{elas}=\frac{\mu\theta}{L}(J+J_c), \tag{20}$$

where J is the cross-section polar moment of inertia J_c is the microstructure-dependent polar moment of inertia (Tong et al. 2004):

$$J=\begin{cases} \dfrac{\pi t^4}{2} & \text{circular} \\ \dfrac{tw^3}{3}\left[1-\dfrac{192w}{\pi^5 t}\displaystyle\sum_{n=1}^{\infty}\dfrac{1}{(2n-1)^5}\tanh\left[\dfrac{(2n-1)\pi t}{2w}\right]\right] & \text{rectangular} \end{cases}, \tag{21}$$

$$J_c=\begin{cases} 3Al^2 & \text{circular} \\ 3Al^2+\dfrac{tw(w^2+t^2)}{12}+\displaystyle\iint_A\left(X\frac{\partial\Phi}{\partial Y}-Y\frac{\partial\Phi}{\partial X}\right)\mathrm{d}X\mathrm{d}Y-J & \text{rectangular} \end{cases}. \tag{22}$$

In the above relation, A, t and w are the area, thickness and width of the beam cross-section, respectively. Furthermore, Φ is the warping function which is determined numerically. It should be noted that J_c is microstructure-dependent, i.e., it is a function of the length scale parameter (l). For two typical cross section geometries e.g., square and circular the non-dimensional parameter J_c/J is plotted versus l/t in Fig. 2.

Now by substituting Eqs. (9), (15) and (20) into (16) we have:

$$\begin{aligned} &\frac{2\Theta\theta_{\max}\mu\mathrm{J}\left(1+\frac{\mathrm{I}_c}{J}\right)}{L}-\frac{\varepsilon\mathrm{b}\mathrm{V}^2}{2\Theta^2\theta_{\max}^2}\left\{\frac{1-\Delta}{1-\Delta-\beta\Theta}-\frac{1-\Delta}{1-\Delta-\alpha\Theta}\right. \\ &\left.+\ln\left[\frac{1-\Delta-\beta\Theta}{1-\Delta-\alpha\Theta}\right]\right\} \\ &-\frac{\pi^2\hbar\mathrm{c}\mathrm{b}a^2}{1440\mathrm{D}^4(1-\Delta)^3(1-\Delta-\Theta)^3}\{((1-\Delta)(3-3\Delta-\Theta)) \\ &-\frac{8c[2(1-\Delta)^2+(2-2\Delta-\Theta)^2]}{3D\omega_p(1-\Delta-\Theta)} \\ &\left.+\frac{72c^2}{D^2\omega_p^2}\left(\frac{D-\delta}{1-\Delta-\Theta}+\frac{\Theta^2(5-5\Delta-\Theta)}{10(1-\Delta)(1-\Delta-\Theta)^2}\right)\right\}=0. \end{aligned} \tag{23}$$

Equation (23) expresses the torsion equilibrium of the nanobeams and relates rotation and deflection of the main-plate to the external voltage as well as the microstructure parameter and Casimir force.

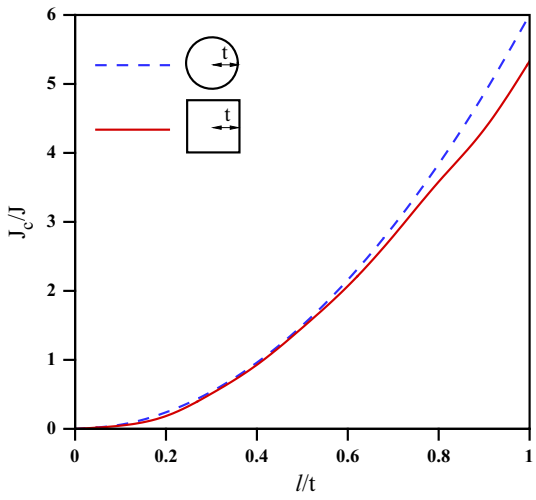

Fig. 2 Variation of J_c/J as a function of microstructure parameter (l/t) for different cross sections

3.4 Bending equilibrium of the beam

To find the bending equilibrium governing equation of the main plate, one can use an energy approach. For this, first the components of the displacement vector for bending beam is expressed as (Dym and Shames 1984)

$$\begin{aligned} &u_1(Z) = 0 \\ &u_2(Z) = v(Z) \\ &u_3(Z) = -Y\frac{\partial v(Z)}{\partial Z}, \end{aligned} \tag{24}$$

where u_1, u_2 and u_3 are the displacement along the X, Y and Z direction, respectively.

By substituting this displacement field in Eqs. (2a)–(2e) and substituting the results in Eq. (1) the bending elastic energy, U_b, can be determined as:

$$U_b = \frac{1}{2}\int_0^L (EI + \mu A I^2)\left(\frac{d^2v}{dZ^2}\right)^2 dZ. \tag{25}$$

The stretching energy stored in the beam (U_{ST}) can be written as:

$$U_{ST} = \frac{BHE}{8L}\left[\int_0^L \left(\frac{dv}{dZ}\right)^2 dZ^2\right]. \tag{26}$$

And finally, the work by the external forces (W_e) can be obtained as:

$$W_e = \int_0^{v=v(L)} \left(\frac{1}{2}[F_{Cas} + F_{elec}]\right) dw. \tag{27}$$

A trial solution for deflection of the nano-beam which satisfies the boundary conditions can be selected as:

$$v(Z) = \delta\left[\frac{1}{2} - \frac{1}{2}\cos\left(\frac{\pi Z}{L}\right)\right]. \tag{28}$$

By substituting Eq. (28) in Eqs. (25), (26) and (27), the total energy of system, Π, can be written as:

$$\begin{aligned} \Pi = U_b + U_{ST} - W_e = \frac{\pi^4(EI + \mu A I^2)}{16L^3}\delta^2 + \frac{AE\pi^4}{512L^3}\delta^4 \\ - \frac{1}{2}\int_0^{\delta} (F_{Cas} + F_{elec})dv. \end{aligned} \tag{29}$$

By imposing the minimum energy for equilibrium, i.e., $\frac{\partial \Pi}{\partial \delta} = 0$, we obtain relations (30) for nano-beam

$$\frac{1}{2}F_{elec} + \frac{1}{2}F_{Cas} - \frac{\pi^4(EI + \mu A I^2)}{8L^3}\delta - \frac{AE\pi^4}{128L^3}\delta^3 = 0. \tag{30}$$

Now by substituting Eqs. (6), (12) in Eq. (30) and using non-dimensional parameter we have:

$$\begin{aligned} &\frac{\varepsilon V^2 b}{4\theta_{\max}\Theta D}\left\{\frac{1}{1-\Delta-\beta\Theta} - \frac{1}{1-\Delta-\alpha\Theta}\right\} \\ &+ \frac{\pi^2\hbar cab}{2880D^4(1-\Delta)^3(1-\Delta-\Theta)^3}\left\{2\Theta^2 + 6(1-\Delta)(1-\Delta-\Theta)\right. \\ &- \frac{8c(2-2\Delta-\Theta)}{D\omega_p}\left[\frac{1-\Delta-\Theta}{1-\Delta} + \frac{1-\Delta}{1-\Delta-\Theta}\right] \\ &\left.+ \frac{144c^2}{D^2\omega_p^2}\left[\frac{1-\Delta-\Theta}{1-\Delta} + \frac{\Theta}{1-\Delta-\Theta} + \frac{\Theta^4}{5(1-\Delta)^2(1-\Delta-\Theta)^2}\right]\right\} \\ &- \frac{\pi^4 D(EI + \mu A I^2)}{8L^3}\Delta - \frac{AE\pi^4 D^3}{128L^3}\Delta^3 = 0. \end{aligned} \tag{31}$$

Equation (31) expresses the bending equilibrium of the nanobeams and relates the rotation and deflection of the main-plate to the applied voltage, microstructure parameter and Casimir attraction.

3.5 Solving the equilibrium equations

To determine the instability parameters of the mirror, Eqs. (29) and (31) can be rearranged in the new following forms:

$$\Xi_1(\Theta, \Delta) = \bar{V} = \left\{\frac{(1 + \frac{J_e}{J})\Theta^4 - \frac{\xi\Theta^3}{(1-\Delta)^3(1-\Delta-\Theta)^3}\left\{((1-\Delta)(3-3\Delta-\Theta)) - \frac{8\lambda[2(1-\Delta)^2 + (2-2\Delta-\Theta)^2]}{3(1-\Delta-\Theta)} + 72\lambda^2\left(\frac{1-\Delta}{1-\Delta-\Theta} + \frac{\Theta^2(5-5\Delta-\Theta)}{10(1-\Delta)(1-\Delta-\Theta)^2}\right)\right\}}{\frac{\Theta(1-\Delta)}{1-\Delta-\beta\Theta} - \frac{\Theta(1-\Delta)}{1-\Delta-\alpha\Theta} + \Theta\ln\left(\frac{1-\Delta-\beta\Theta}{1-\Delta-\alpha\Theta}\right)}\right\}^{\frac{1}{2}} \tag{32}$$

$$\Xi_2(\Theta, \Delta) = \Xi_1(\Theta, \Delta) - \left\{\frac{K^2(1 + \frac{6}{1+v}(\frac{l}{t})^2)\Delta\Theta^2 + K^2(1 + \frac{6}{1+v}(\frac{l}{t})^2)\eta\Delta^3\Theta^2 - \frac{\xi\Theta\left\{2\Theta^2 + 6(1-\Delta)(1-\Delta-\Theta) - 8\lambda(2-2\Delta-\Theta)[\frac{1-\Delta-\Theta}{1-\Delta} + \frac{1-\Delta}{1-\Delta-\Theta}] + 144\lambda^2\left[\frac{1-\Delta-\Theta}{1-\Delta} + \frac{\Theta}{1-\Delta-\Theta} + \frac{\Theta^4}{5(1-\Delta)^2(1-\Delta-\Theta)^2}\right]\right\}}{(1-\Delta)^3(1-\Delta-\Theta)^3}}{\frac{\Theta}{1-\Delta-\beta\Theta} - \frac{\Theta}{1-\Delta-\alpha\Theta} - \lambda\left(\frac{1-\Delta}{1-\Delta-\beta\Theta} - \frac{1-\Delta}{1-\Delta-\alpha\Theta} + \ln\left(\frac{1-\Delta-\beta\Theta}{1-\Delta-\alpha\Theta}\right)\right)}\right\}^{\frac{1}{2}} = 0, \tag{33}$$

where

$$\xi = \frac{\pi^2 \hbar c b L}{2880\theta_{\max}^3 D^2 \mu J}, \tag{34a}$$

$$\lambda = \frac{c}{\omega_p D}, \tag{34b}$$

$$\eta = \frac{AED^2}{16.683EI}, \tag{34c}$$

$$\overline{V}^2 = \frac{\varepsilon V^2 bL}{4\mu J \theta_{\max}^3}, \tag{34d}$$

$$K = \frac{\pi^2 D}{\theta_{\max} L}\sqrt{\frac{EI}{8\mu J}}. \tag{34e}$$

The parameter K show the ratio of bending stiffness to torsion stiffness of the nanobeam. The torsion mode is dominant in the case of large values of K while the bending mode is dominant for low K values.Equations (32) and (33) are solved to determine the rotation (Θ) and deflection (Δ) of the mirror for any applied voltage difference ($\bar{V}$). According to the implicit function theorem (Daqaq et al. 2008), the pull-in point should be satisfied the following condition:

$$\begin{vmatrix} \frac{\partial \Xi_1}{\partial \Theta}(\Theta_{PI}, \Delta_{PI}) & \frac{\partial \Xi_1}{\partial \Delta}(\Theta_{PI}, \Delta_{PI}) \\ \frac{\partial\ \Xi_2}{\partial \Theta}(\Theta_{PI}, \Delta_{PI}) & \frac{\partial\ \Xi_2}{\partial \Delta}(\Theta_{PI}, \Delta_{PI}) \end{vmatrix} = 0, \tag{35}$$
$$\Xi_2(\Theta_{PI}, \Delta_{PI}) = 0.$$

From Eq. (35), the instability parameters of the mirror which defined as Θ, Δ at the pull-in point (Θ_{PI} and Δ_{PI}) are determined as a function of the electrode geometrical parameters (α and β), coupling parameter (K) and the length scale parameters (l). Finally, by substituting the obtained Θ_{PI} and Δ_{PI} in Eq. (22) $\bar{V}$ at the pull-in point ($\bar{V}_{PI}$) is determined.

4 Result and discussion

4.1 Bending/torsion coupled instability

Influence of coupling ratio (K) and geometrical parameter (β) on the pull-in behavior of typical micro-mirror is shown in Fig. 3. As seen, the pull-in behavior depends on the value of the coupling parameter (K). For systems with $K \geq 15$, the instability angle is very close to the results of pure torsion model ($K = \infty$). Interestingly, if both bending and torsion stiffness are considerable, an increase–decrease trend can be observed in Θ_{PI}–β curves. It is due to the conquering of the bending pull-in mode over the torsion mode. Moreover, the instability voltage determined by the 2-DOF model is lower than of the 1-DOF model.

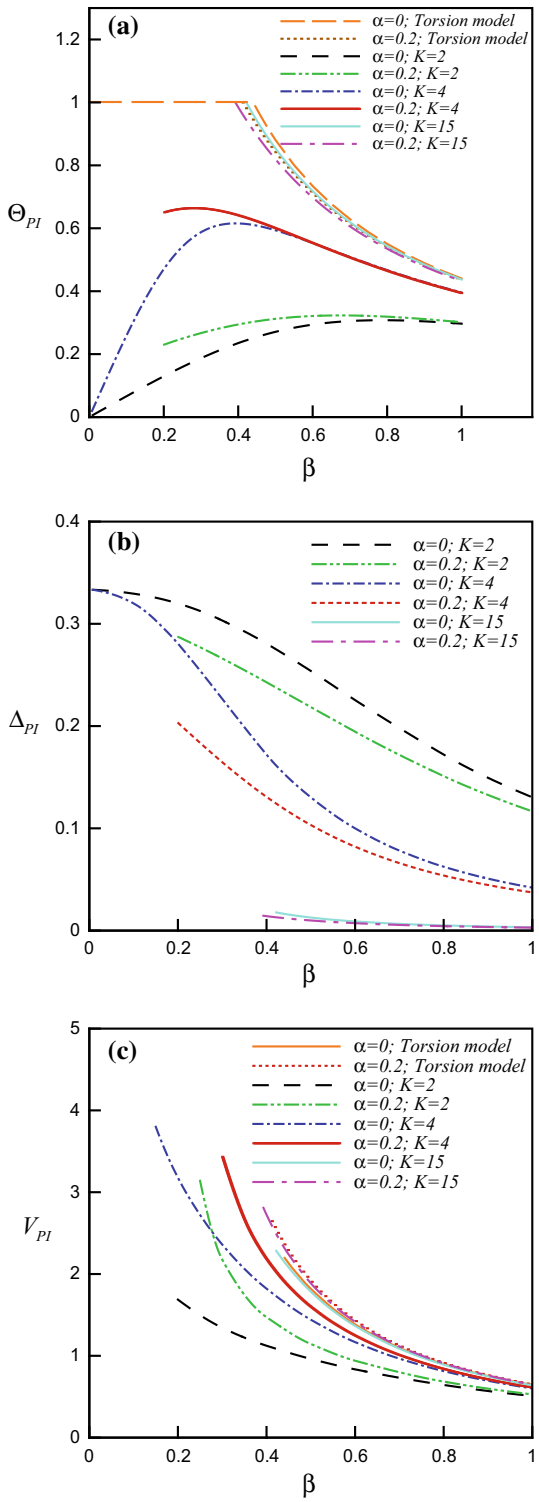

Fig. 3 Impact of geometry parameter (β) and coupling ration (K) on the pull-in parameters **a** pull-in angle, **b** pull-in displacement, and **c** pull-in voltage

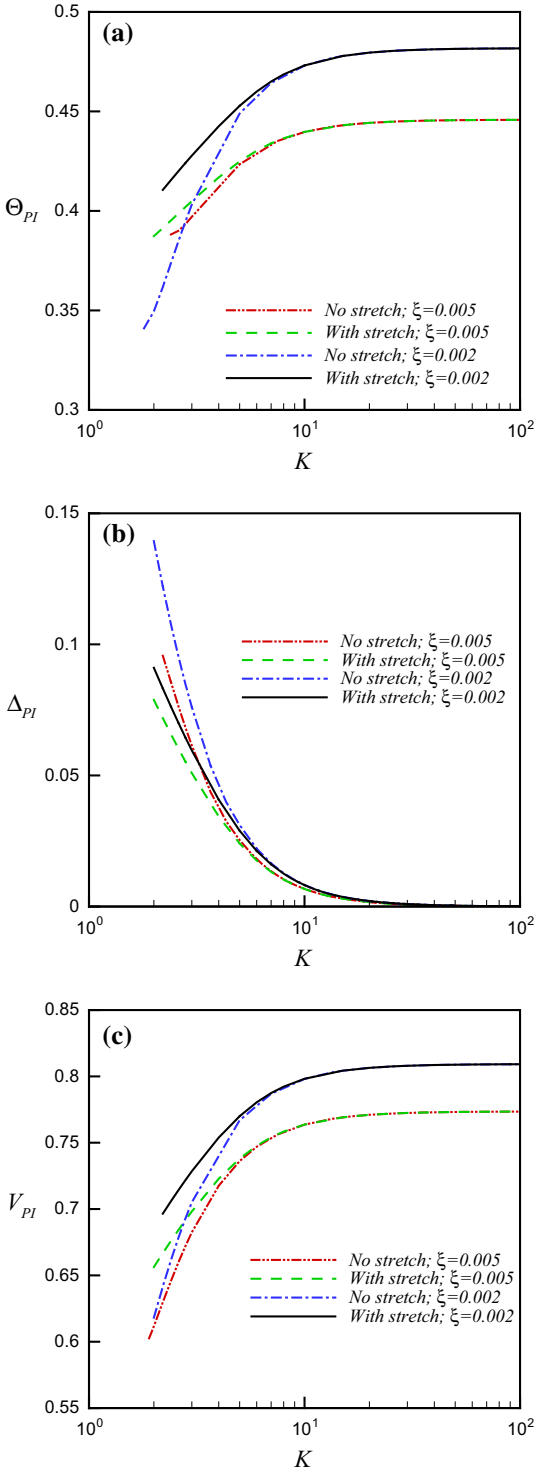

Fig. 4 Influence of considering stretching on **a** pull-in angle, **b** pull-in displacement, and **c** pull-voltage for different values of Casimir force

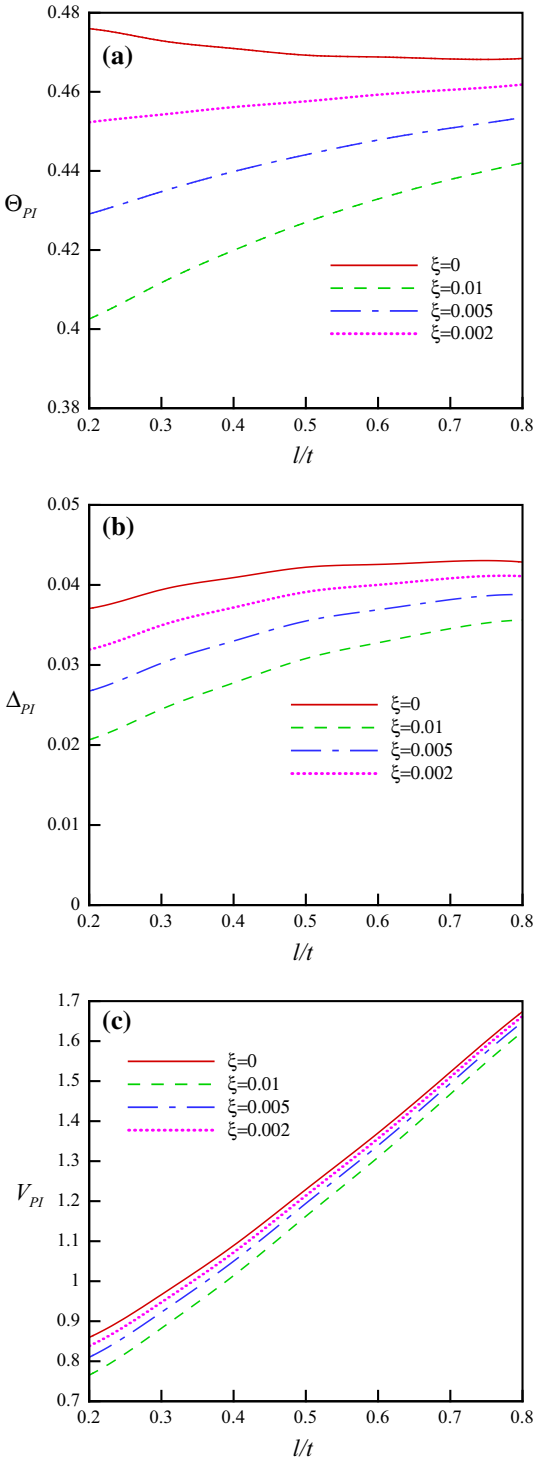

Fig. 5 Influence of microstructure and Casimir force on the pull-in parameters **a** pull-in angle, **b** pull-in displacement, and **c** pull-voltage

4.2 Stretching

For nanobeams with clamped ends, the beam stretching results in the axial strain and stress. The two terms on the right-hand side of Eq. (33) are associated with the two different deformation modes. The former, that is linear in Δ, is due to the bending deformation while the later, that is proportional to Δ^3, is due to the beam stretching.

Figure 4 shows the influence of stretching on the pull-in parameters of the mirror. This figure reveals that the stretching slightly increases the pull-in voltage of the mirror. On the other hand, a comparison between Fig. (4a–c) reveals that although the stretching is highly important for determining pull-in deflection, it can be neglected for calculating the values of pull-in voltage and pull-in angle. This figure demonstrates that the stretching effect is more significant for low values of K i.e., bending mode of instability while it can be ignored for torsional pull-in mode.

4.3 Microstructure effect

Figure 5 illustrates the impact of length scale parameter on the instability behavior of the typical mirror. As seen microstructure effect enhances the instability threshold of the nano-mirrors. The microstructure dependency increases the pull-in voltage and pull in deflection of the mirror and reduces the pull-in angle. The pull-in voltage calculated by the presented microstructure dependent model is higher than that determined by the classical theory. In addition, this stiffening trend is more important for larger l/t values. Figure 5 reveals that when the thickness of the torsional beam is in the order of the material length scale parameter, classic model might not be precise enough for determining the pull-in parameters of miniature mirror fabricated from microstructure-dependent materials.

The effects of microstructure as well as Casimir force on the instability of a typical scanner are demonstrated in Fig. 6 where the variation of the instability parameters is presented versus the coupling ratio (K). As seen, the Casimir force has a softening effect and reduces the pull-in voltage. While microstructure effect increases the pull-in voltage, Casimir force reduces the instability threshold of the system.

When the initial gap becomes sufficiently small, the freestanding nano-mirror adheres the ground even without an applied voltage. This undesirable stiction is due to the presence of the Casimir forces. The critical values of the Casimir force at the instability threshold are very important in nano-mirror design. Figure 7 shows the influence of microstructure parameter on the critical values of Casimir force for freestanding nano-mirror and its related pull-in displacement and pull-in angle. This figure reveals that while the critical values of Casimir force increase by increasing the size parameter, the pull-in deflection and pull-in angle of freestanding nano-mirror don't change significantly by increasing the size parameter.

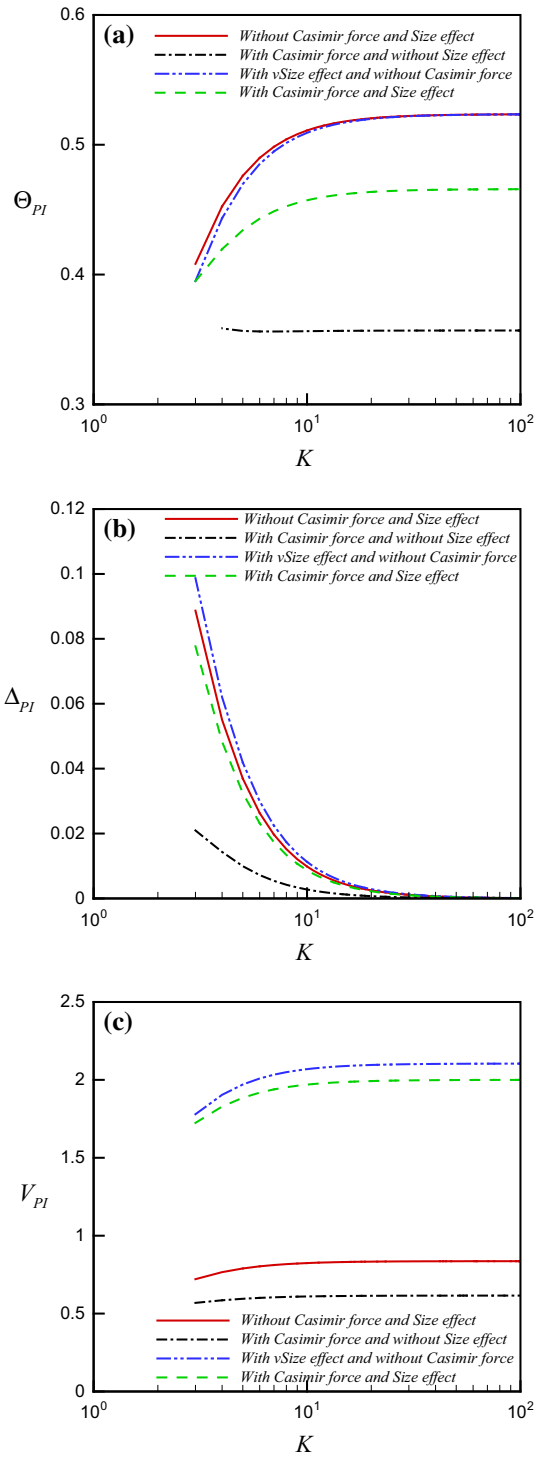

Fig. 6 Variation of **a** pull-in angle, **b** pull-in displacement, and **c** pull-in voltage vs. K parameter ($\alpha = 0.06$ and $\beta = 0.84$)

4.4 Validation

Figure 8 compares the pull-in voltage predicted by the presented model with those obtained experimentally by (Zhang et al. 2001). As seen while the classical model ($l = 0$) can't predict the pull-in voltage accurately the results of presented size dependent model are very close to experimental data.

Huang et al. (2004) experimentally evaluated the pull-in voltage of a nano-mirror. The material properties and

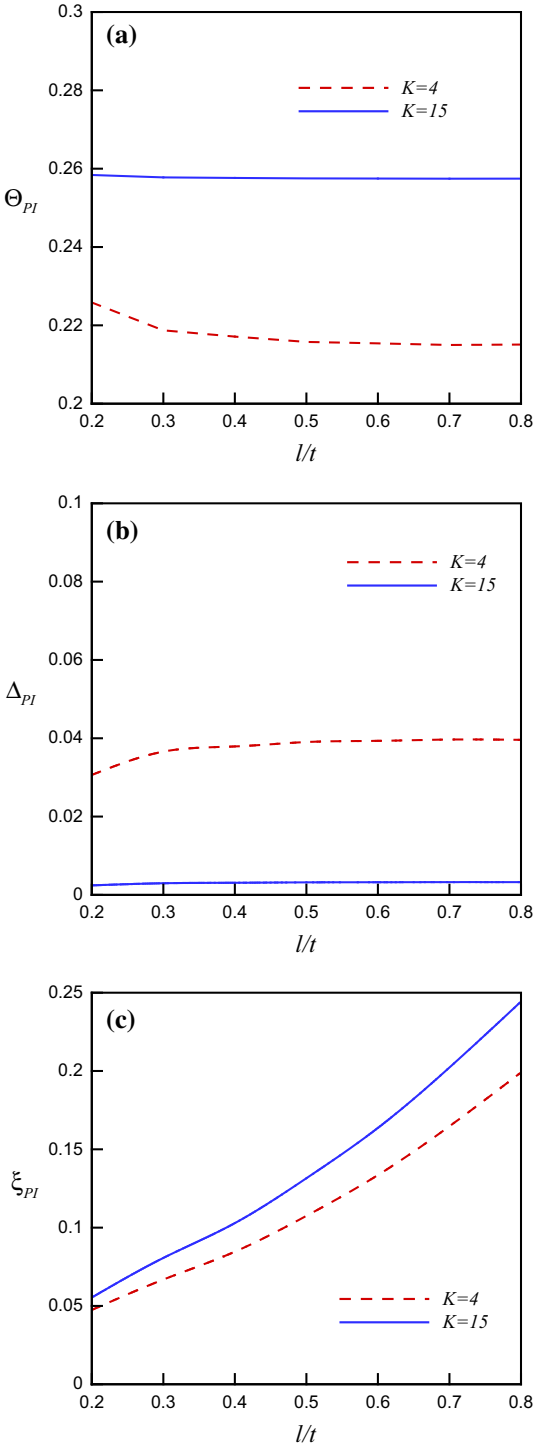

Fig. 7 Influence of microstructure on the critical values of free-standing nano-mirror at pull-in point **a** pull-in angle, **b** pull-in displacement, and **c** critical Casimir force

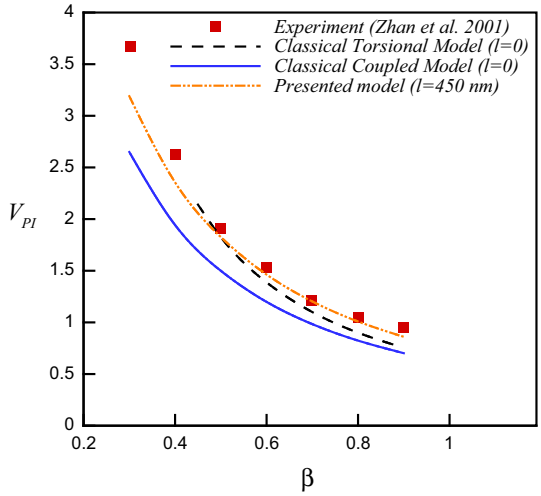

Fig. 8 Comparison the pull-in voltage calculate by theoretical models with experimental results

Table 1 Material properties and geometrical parameters of the nano-mirror of Table 2 (Huang et al. 2004)

Items	Value
Material properties	
Young's modulus, E (Gpa)	169
Poisson's ratio, υ	0.29
Geometrical parameters	
Mirror width, a (μm)	100
Mirror length, b (μm)	100
Torsional beam length, L (μm)	65
Torsional beam width, w (μm)	1.55
Torsional beam thickness, t (μm)	1.5
Gap, D (μm)	2.75
Electrode inner width, a_1 (μm)	6
Electrode outer width, a_2 (μm)	84

Table 2 Comparison between the pull-in parameters obtained by the experimental results and those of different theories ($K = 3.243$)

Model	V_{PI} (V)	Θ_{PI}	Δ_{PI}
Experiment (Huang et al. 2004)	17.4	0.4198	0.0778
1-DOF torsion model (Huang et al. 2004)	20.1	0.5236	–
Rezazadeh et al. (2007)	17.5	0.4224	0.0763
Beni et al. (2011)	17.55	0.4207	0.0785
Presented model (l = 150 nm)	18.17	0.4270	0.0752

geometrical parameters of studied mirror are presented in Table 1. Table 2 compares the pull-in parameters depict by presented model and the experimental results (Huang et al. 2004) as well as models (Rezazadeh et al. 2007; Beni et al. 2011). This table implies that the instability parameters determined by the proposed model are in good agreement with those of experimental. In particular, the pull-in parameters determined by the presented model are in closer to the experimental values than the 1-DOF torsion model. Figure 8

and Table 2 demonstrate that the presented model is in better agreement with experiments in comparison with the 1-DOF torsional and classical 2-DOF models. Indeed, both of these models present uniform trends i.e., softening (for 2-DOF model) or hardening (for 1-DOF models). However, the presented model is able to predict both hardening

5 Conclusions

A microstructure dependent model has been presented to investigate the coupled torsion-bending pull-in instability of nano-mirror. The governing equations are derived incorporating the influence of corrected Casimir force with the consideration of the finite conductivity of interacting surfaces. It is found that the pull-in voltage decreases with decreasing coupling ratio. Neglecting the microstructure effect may cause major error in simulation of the system. Increasing the microstructure effect causes a hardening effect i.e., decreases the instability voltage. Impact of microstructure dependency on instability voltage of the nano-mirror depends on coupling ratio and the conquering bending mode over torsion mode. In addition, the Casimir force reduces the instability threshold of the system and has a softening effect. Rather than the microstructure dependency and Casimir force the stretching of supported beam is studied. It is found that, although the stretching is highly important for determining pull-in deflection, it can be neglected for calculating the values of pull-in voltage and pull-in angle. While the stretching effect is crucial for bending mode of instability it can be ignored for torsional pull-in mode. Modelling the instability behavior of freestanding nano-mirror reveals that, while the critical values of Casimir force increase by increasing the size parameter, the pull-in deflection and pull-in angle of freestanding nano-mirror don't change significantly by increasing the size parameter. It is demonstrated that the gap between the experiment and theory can be reduced by using the presented size-dependent model. The developed model is able to predict the experimental results more accurately than the previous classic models.

References

Abdi J, Koochi A, Kazemi AS, Abadyan M (2011) Modeling the effects of size dependence and dispersion forces on the pull-in instability of electrostatic cantilever NEMS using modified couple stress theory. Smart Mater Struct 2 20(5):055011

Akgoz B, Civalek O (2011a) Application of strain gradient elasticity theory for buckling analysis of protein microtubules. Curr Appl Phys 11:1133–1138

Akgoz B, Civalek O (2011b) Strain gradient elasticity and modified couple stress models for buckling analysis of axially loaded micro-scaled beams. Int J Eng Sci 49:1268–1280

Akgoz B, Civalek O (2014) Longitudinal vibration analysis for microbars based on strain gradient elasticity theory. J Vibration Control 20(4):606–616

Akgoz B, Civalek O (2015a) A novel microstructure-dependent shear deformable beam model. Int J Mech Sci 99:10–20

Akgoz B, Civalek O (2015b) A microstructure-dependent sinusoidal plate model based on the strain gradient elasticity theory. Acta Mech 226:2277–2294

Akgöz B, Civalek O (2014) Shear deformation beam models for functionally graded microbeams with new shear correction factors. Composite Struct 112:214–225

Batra RC, Porfiri M, Spinello D (2007) Effects of Casimir force on pull-in instability in micromembranes. Eur Phys Lett 77:20010

Beni YT (2015) Using modified couple stress theory to investigate the size-dependent instability of rotational nano-actuator under van der Waals force. APJES 3:42–47

Beni YT, Abadyan M (2013) Use of strain gradient theory for modeling the size-dependent pull-in of rotational nano-mirror in the presence of molecular force. Int J Modern Phys B 27:1350083

Beni YT, Abadyan M, Koochi A (2011) Effect of the Casimir attraction on the torsion/bending coupled instability of electrostatic nano-actuators. Phys Scripta 84:065801

Beni YT, Koochi A, Kazemi AS, Abadyan M (2012) Modeling the influence of surface effect and molecular force on pull-in voltage of rotational nano–micro mirror using 2-DOF model. Can J Phys 90:963–974

Bezerra VB, Klimchitskaya GL, Romero C (1997) Casimir force between a flat plate and a spherical lens: application to the results of a new experiment. Modern Phys Lett A 12:2613–2622

Bochobza-Degani O, Nemirovsky Y (2002) Modeling the pull-in parameters of electrostatic actuators with a novel lumped two degrees of freedom pull-in model. Sensor Actuator A 97:569–578

Buks E, Roukes ML (2001) Stiction, adhesion energy, and the Casimir effect in micromechanical systems. Phys Rev B 63:033402

Capasso F, Munday JN, Iannuzzi D, Chen HB (2007) Casimir forces and quantum electrodynamical torques: physics and nanomechanics. IEEE J Select Topics Quantum Electron 13:400–414

Daqaq MF, Abdel-Rahman EM, Nayfeh AH (2008) Towards a stable low-voltage torsional microscanner. Microsys Tech 14:725–737

Degani O, Nemirovsky Y (2002) Design considerations of rectangular electrostatic torsion actuators based on new analytical pull-in expressions. J Microelectromech Sys 11:20–26

Degani O, Socher E, Lipson A, Leitner T, Setter DJ, Kaldor S, Nemirovsky Y (1998) Pull-in study of an electrostatic torsion microactuator. J Microelectromech Sys 7(4):373–379

Duan JS, Rach R (2013) A pull-in parameter analysis for the cantilever NEMS actuator model including surface energy, fringing field and Casimir effects. Int J Solid Struct 50:3511–3518

Dym CL, Shames IH (1984) Solid mechanics: a variational approach. Railway Publishing House, Beijing

Eringen AC (1983) On differential equations of nonlocal elasticity and solutions of screw dislocation and surface waves. J Appl Phys 54:4703–4710

Fleck NA, Muller GM, Ashby MF, Hutchinson JW (1994) Strain gradient plasticity: theory and experiment. Acta Metall Mater 42:475–487

Ford JE, Aksyuk VA, Bishop DJ, Walker JA (1999) Wavelength add-drop switching using tilting micromirrors. J Lightwave Tech 17:904

Guo JG, Zhao YP (2004) Influence of van der Waals and Casimir forces on electrostatic torsional actuators. J Microelectromech Sys 13(6):1027–1035

Guo JG, Zhao YP (2006) Dynamic stability of electrostatic torsional actuators with van der Waals effect. Int J Solid Struct 43:675–685

Hargreaves C M (1965) Corrections to the related dispersion force between metal bodies. Proceedings of the Koninklijke Nederlandse Akademie van Wetenschappen

Huang JM, Liu AQ, Deng ZL, Zhang QX, Ahn J, Asundi A (2004) An approach to the coupling effect between torsion and bending for electrostatic torsional micromirrors. Sensor Actuator A 115:159–167

Koochi A, Farrokhabadi A, Abadyan M (2015) Modeling the size dependent instability of NEMS sensor/actuator made of nanowire with circular cross-section. Microsys Tech 21:355–364

Lam DCC, Yang F, Chong ACM, Wang J, Tong P (2003) Experiments and theory in strain gradient elasticity. J Mech Phys Solid 51(8):1477–1508

Lambrecht A, Jaekel MT, Reynaud S (1997) The Casimir force for passive mirrors. Phys Lett A 225:188–194

Lamoreaux SK (1999) Calculation of the Casimir force between imperfectly conducting plates. Phys Rev A 59:R3149

Lamoreaux SK (2004) The Casimir force: background, experiments, and applications. Rep Prog Phys 68:201

Lin WH, Zhao YP (2003) Dynamics behavior of nanoscale electrostatic actuators. Chin Phys Lett 20:2070–2073

Lin WH, Zhao YP (2005) Casimir effect on the pull-in parameters of nanometer switches. Microsys Tech 11:80–85

Lin WH, Zhao YP (2007a) Influence of damping on the dynamical behavior of the electrostatic parallel-plate and torsional actuators with intermolecular forces. Sensors 7:3012–3026

Lin WH, Zhao YP (2007b) Stability and bifurcation behaviour of electrostatic torsional NEMS varactor influenced by dispersion forces. J Phys D 40:1649

Miandoab EM, Yousefi-Koma A, Pishkenari HN (2015) Nonlocal and strain gradient based model for electrostatically actuated silicon nano-beams. Microsys Tech 21:457–464

Moeenfard H, Ahmadian MT (2013) Analytical modeling of bending effect on the torsional response of electrostatically actuated micromirrors. Optik 124:1278–1286

Moeenfard H, Darvishian A, Zohoor H, Ahmadian MT (2012) Characterization of the static behavior of micromirrors under the effect of capillary force, an analytical approach. J Mech Eng Sci 226:2361–2372

Nemirovsky Y, Bochobza-Degani O (2001) A methodology and model for the pull-in parameters of electrostatic actuators. J Microelectromech Sys 10:601–615

Noruzifar E, Emig T, Zandi R (2011) Universality versus material dependence of fluctuation forces between metallic wires. Phys Rev A 84:042501

Peng JS, Yang L, Yang J (2015) Size effect on the dynamic analysis of electrostatically actuated micro-actuators. Microsys Tech. doi:10.1007/s00542-015-2788-9

Rahaeifard M, Kahrobaiyan MH, Asghari M, Ahmadian MT (2011) Static pull-in analysis of microcantilevers based on the modified couple stress theory. Sens Actuators A 171:370–374

Rezazadeh G, Khatami F, Tahmasebi A (2007) Investigation of the torsion and bending effects on static stability of electrostatic torsional micromirrors. Microsys Tech 13:715–722

Rodriguez AW, Capasso F, Johnson SG (2011) The Casimir effect in microstructured geometries. Nat Photonics 5:211–221

Sedighi HM (2014) The influence of small scale on the pull-in behavior of nonlocal nanobridges considering surface effect, Casimir and van der Waals attractions. Int J Appl Mech 6:1450030

Sedighi HM, Koochi A, Abadyan M (2014) Modeling the size-dependent static and dynamic pull-in instability of Cantilever nanoactuator based on strain gradient theory. Int J Appl Mech 6:1450055

Tong P, Yang F, Lam DC, Wang J (2004) Size effects of hair-sized structures–torsion. In Key Eng Mater 261:11–22

Toshiyoshi H, Fujita H (1996) Electrostatic micro torsion mirrors for an optical switch matrix. J Microelectromech Sys 5:231–237

Tsiatas GC, Katsikadelis JT (2011) A new microstructure-dependent Saint–Venant torsion model based on a modified couple stress theory. Eur J Mech A 30:741–747

Wen-Hui L, Ya-Pu Z (2003) Dynamic behaviour of nanoscale electrostatic actuators. Chin Phys Lett 20:2070

Xiao Z, Wu X, Peng W, Farmer KR (2001) An angle-based design approach for rectangular electrostatic torsion actuators. J Microelectromech Sys 10:561–568

Yang F, Chong ACM, Lam DCC, Tong P (2002) Couple stress based strain gradient theory for elasticity. Int J Solid Struct 39:2731–2743

Zhang XM, Chau FS, Quan C, Lam YL, Liu AQ (2001) A study of the static characteristics of a torsional micromirror. Sens Actuator A 90:73–81

Zhao JP, Chen HL, Huang JM, Liu AQ (2005) A study of dynamic characteristics and simulation of MEMS torsional micromirrors. Sens Actuator A 120:199–210